Quaternary Science Reviews 103 (2014) 81–90

Contents lists available at ScienceDirect

Quaternary Science Reviews

journal homepage: www.elsevier.com/locate/quascirev

Assessing the strength of the monsoon during the late Pleistocene in southwestern United States

Luz M. Cisneros-Dozal [a, *], Yongsong Huang [b], Jeffrey M. Heikoop [a], Peter J. Fawcett [c], Julianna Fessenden [a], R. Scott Anderson [e, f], Philip A. Meyers [g], Toti Larson [a, 1], George Perkins [a], Jaime Toney [b, 2], Josef P. Werne [d, 3], Fraser Goff [c], Giday WoldeGabriel [a], Craig D. Allen [h], Melissa A. Berke [d, 4]

[a] Earth and Environmental Sciences Division, EES-14, Los Alamos National Laboratory, Los Alamos, NM 87545, USA
[b] Department of Geological Sciences, Brown University, Providence, RI 02912, USA
[c] Department of Earth & Planetary Sciences, University of New Mexico, Albuquerque, NM 87131, USA
[d] Large Lakes Observatory, University of Minnesota Duluth, Duluth, MN 55812, USA
[e] School of Earth Sciences and Environmental Sustainability, Northern Arizona University, Flagstaff, AZ 86011, USA
[f] Laboratory of Paleoecology, Bilby Research Center, Northern Arizona University, Flagstaff, AZ 86011, USA
[g] Department of Earth and Environmental Sciences, The University of Michigan, Ann Arbor, MI 48109, USA
[h] U.S.G.S. Fort Collins Science Center, Jemez Mountains Field Station, Los Alamos, NM 87544, USA

ARTICLE INFO

Article history:
Received 10 February 2014
Received in revised form
7 July 2014
Accepted 13 August 2014
Available online

Keywords:
Monsoonal precipitation
Hydrogen isotope
Leaf plant waxes
Southwestern US
Drought

ABSTRACT

Improved predictions of drought require an understanding of natural and human-induced climate variability. Long-term records across glacial–interglacial cycles provide the natural component of variability, however few such records exist for the southwestern United States (US) and quantitative or semi-quantitative records of precipitation are absent. Here we use the hydrogen isotope (δD) value of C_{28} *n*-alkanoic acid in lacustrine sediments of Pleistocene age to reconstruct δD values of precipitation in northern New Mexico over two glacial–interglacial cycles (~550,000–360,000 years before present) and obtain a record of monsoon strength. Overall, reconstructed δD values range from −53.8‰ to −94.4‰, with a mean value of −77.5 ± 8‰. Remarkably, this variation falls within the measured present-day summer monsoonal and winter weighted means (−50.3 ± 3‰ and −106.4 ± 20‰ respectively), suggesting that processes similar to those of present time also controlled precipitation during Marine Isotope Stage (MIS) 13 to 10. Using the δD summer monsoonal and winter mean values as end-members, we interpret our reconstructed δD record of precipitation as a direct, and semi-quantitative, indicator of monsoon strength during MIS 13 to 10. Interglacial periods were characterized by greater monsoon strength but also greater variability compared to glacial periods. Pronounced cycles in the strength of the monsoon occurred during interglacial periods and in general were positively correlated with maximum mean annual temperatures. Our estimates of monsoon strength are supported by independent proxies of ecosystem productivity, namely, TOC, $\delta^{13}C$ of TOC and Si/Ti ratio and warm pollen taxa *Juniperus* and *Quercus*. Interglacial variability in the strength of the monsoon resembles a response to the land-sea surface temperature contrast (LSTC) except for the early part of MIS 11. During this period, LSTC would have remained relatively strong while monsoonal strength decreased to a minimum. This minimum occurred following the warmest interval of MIS 11, suggesting a more complex driving of monsoon strength during warm periods. In addition, this period of monsoon minimum coincided with a core section of mud-cracked sediments that suggest low monsoonal precipitation was an important factor in the onset of drought. Our estimates of monsoon strength represent a record of natural variability

* Corresponding author. Present address: Natural Environment Research Council Radiocarbon Facility – East Kilbride, Scottish Universities Environmental Research Centre, East Kilbride, G75 0QF, UK. Tel.: +44 (0)1355 260037; fax: +44 (0) 1355 229829.
E-mail address: Malu.Cisneros@glasgow.ac.uk (L.M. Cisneros-Dozal).
[1] Present address: Department of Geological Sciences, The University of Texas at Austin, Austin, TX 78712, USA.
[2] Present address: School of Geographical and Earth Sciences, University of Glasgow, Glasgow, G12 8QQ, UK.
[3] Present address: Department of Geology & Planetary Science, University of Pittsburgh, Pittsburgh, PA 15260, USA.
[4] Present address: University of Notre Dame, Dept. of Civil & Environmental Engineering & Earth Sciences, Notre Dame, IN 46556, USA.

http://dx.doi.org/10.1016/j.quascirev.2014.08.022
0277-3791/

in the region that is relevant to present time, in particular the variability during interglacial MIS 11, which is considered an analog for the current interglacial. Our results suggest that natural variability can cause significant reductions in monsoonal precipitation with the implication of a potentially adverse effect from sustained warming.

1. Introduction

As a result of human-induced forcing, the arid region of the southwestern US is projected to enter a climate that is drier than what has been observed in the instrumental record (Seager et al., 2007). Ultimately, the combined effect of human-induced forcing and natural forcing will dictate future climate change in the region. One aspect of natural variability is controlled by changes in sea surface temperature. For instance, models suggest that natural variability in tropical Pacific sea surface temperatures (Cook et al., 2007) was a significant source of precipitation variability in the southwest during the last ca 400 years (Seager et al., 2005). However the projected drier climate for the southwestern US is expected to have a more complex forcing involving changes in atmospheric circulation cells (Seager et al., 2007). Whereas all model projections take into account the known past variability available from the instrumental record, these records are limited to ~120 years and thus capture a relatively short period of natural variability. Longer records of precipitation across glacial–interglacial cycles can greatly improve our understanding of natural forcing. In the southwestern US, only a few long-term records exist and these are qualitative in nature (Sears and Clisby, 1952; Winograd et al., 1992; Coplen et al., 1994; Fawcett et al., 2011). Evidence of past dry/wet climate intervals in the southwestern US exists from a chronologically unconstrained lacustrine record retrieved over 60-years ago from the Valles Caldera in northern New Mexico (Sears and Clisby, 1952). A subsequent study on Pleistocene interglacials identified periods of aridity from a new lake core retrieved from Valles Caldera (VC-3 core) (Fawcett et al., 2011). The VC-3 core contained mud-cracked sections, and a multi-proxy analysis provided indirect evidence of significantly reduced precipitation during MIS 13 and 11.

Here we measure compound-specific δD values in the VC-3 core to obtain a semi-quantitative record of monsoonal precipitation during MIS 13 through the onset of MIS 10. We use the δD values of terrestrial plant waxes (C_{28} *n*-alkanoic acid) extracted from the VC-3 core and the modern correlation between the δD value of sedimentary terrestrial plant waxes and that of local precipitation (Hou et al., 2008) to obtain a δD record of precipitation ~550,000–360,000 years before present. In addition, we used the apparent fractionation factor between the δD value of plant leaf waxes and the δD of precipitation (Hou et al., 2008) to obtain a second reconstruction of the δD of precipitation. Using the reconstructed δD of precipitation and a two end-member approach (validated with modern precipitation data), we present a record for the strength of the monsoon during Pleistocene interglacials in northern New Mexico. Our estimates of monsoon strength constitute a record of natural variability in precipitation in the southwestern US that extends considerably longer than the instrumental record and provides direct evidence of semi-quantitative changes not yet available from paleoclimate records. This new record of monsoonal precipitation, particularly during MIS 11, an insolation analog for the current interglacial, will contribute to a better understanding of the mechanisms behind current and future droughts in the region.

2. Materials and methods

2.1. Core sampling

Lacustrine sediments were retrieved from Valles Caldera, New Mexico (35° 52′ N, 106° 28′ W, 2553 m a.s.l.; Fig. 1). Details on the geology of Valles Caldera, the chronology and lithology of the core, pollen, magnetic susceptibility, total organic carbon (TOC), mean annual temperature (MAT), $\delta^{13}C_{TOC}$ and SI/Ti analyses are described elsewhere (Fawcett et al., 2007, 2011). The 82-m VC-3 core is stored at the Limnological Research Center National Lacustrine Core Repository (LacCore) at the University of Minnesota. Sediment

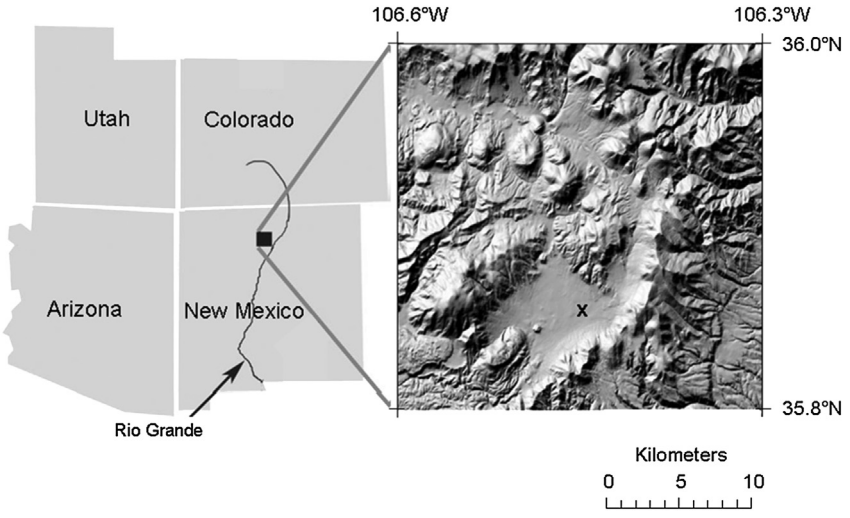

Fig. 1. Location map of Valles Caldera, New Mexico and elevation map showing the drilling location of the lake core (cross).

samples for δD analyses were retrieved from the core at ~0.7–0.9 m resolution (approximately 2100–2700 years). No samples were retrieved from 47 to 43 m depth, which corresponds to a severe desiccation period during MIS 13 that contains extensive mud cracks from 47.5 to 44 m depth. We chose to avoid this section of the core given the likelihood of widespread organic matter degradation (Fawcett et al., 2011) and the resulting loss of the compounds of interest.

2.2. δD analyses of sedimentary material

We measured the δD value of C_{28} *n*-alkanoic acid extracted from the VC-3 core. The amount of sediment extracted for all depths was approximately 1 g (equivalent to ~1 cm of core length, ~30 years). All sediment samples were freeze-dried and homogenized. Sample preparation and δD analyses were performed at Brown University following established protocols (Hou et al., 2008). Briefly, sediment samples were extracted for total lipids using an Accelerated Solvent Extractor (ASE200, Dionex) with dichloromethane:methanol (2:1 v/v). Total lipid extracts were eluted using LC-NH_2 SPE columns (Supelco Supelclean™) into neutral and acid fractions via dichloromethane:isopropyl alcohol and ether with 4% acetic acid, respectively. Acid fractions were methylated using HCl in methanol followed by elution through silica gel columns with hexane and with dichloromethane to remove the hydroxyl fraction and fatty acid methyl esters, respectively. *n*-alkanes and *n*-alkanoic acids (as methyl esters) were quantified and identified by Gas Chromatography–Flame Ionization and Mass Spectrometry Detection. The δD values of *n*-alkanoic acids were determined by Gas Chromatography–Isotope Ratio Mass Spectrometry (GC–IRMS) with a correction for the hydrogen isotopic signature of the added methyl group. The δD composition was determined in duplicate and is reported in the standard δ notation as the per mil deviation (‰) relative to Vienna Standard Mean Ocean Water (VSMOW) standard. δD values were measured on a standard mix of four *n*-acids (C_{16}–C_{28}) and an offset was calculated using hydrogen reference gas with a known isotopic composition. Standards were run after every four samples and drift was corrected as necessary. Precision of the isotopic analyses of the standard mix was ±2‰ throughout the sample run.

2.3. δD analyses of modern precipitation

In order to better understand the variability in the reconstructed δD value of precipitation during the time span of the VC-3 core (see below), we use modern datasets of precipitation (δD values and amount) for the Valles Caldera region. We measured the δD value of modern precipitation in monthly rainfall collections over a 5-yr period (2005–2010) at the Geochemistry and Geomaterials Research Laboratory (GGRL) at Los Alamos National Laboratory (LANL). Rainfall was collected in a bucket under a thin layer of mineral oil to avoid evaporation. δD in water was measured using a GV Instruments Isoprime continuous flow isotope ratio mass spectrometer (GV Instruments, Manchester, UK). δD values are reported using standard δ notation as the per mil deviation (‰) relative to Vienna Standard Mean Ocean Water (VSMOW). δD values were calibrated using in-house standards calibrated to IAEA standards V-SMOW, SLAP and GISP. δD was measured on hydrogen gas derived from chromium reduction of H_2O using a GV Instruments Eurovector Elemental Analyzer. Analytical linearity was monitored and corrected for by analyzing standards after every five samples. Analytical precision on an in-house standard was $<\pm 0.99$‰ on replicate analyses (triplicates).

We estimated the δD values for summer monsoonal (July–September) and winter (December–March) months as the

Table 1
2005–2010 precipitation data for the Valles Caldera region.

Month-year	Precipitation (inches)	δD precipitation (‰)	Month-year	Precipitation (inches)	δD precipitation (‰)
Oct-05	1.1	−73	Jun-08	0.0	na[a]
Nov-05	0.1	−37	Jul-08	2.6	−44
Dec-05	0.0	na[a]	Aug-08	6.0	−51
Jan-06	0.2	na[a]	Sep-08	0.3	−40
Feb-06	0.0	−97	Oct-08	1.4	−70
Mar-06	0.6	−86	Nov-08	0.6	na[a]
Apr-06	0.5	−106	Dec-08	1.6	na[a]
May-06	0.2	−36	Jan-09	0.3	na[a]
Jun-06	1.8	−50	Feb-09	0.0	−77
Jul-06	2.3	−37	Mar-09	1.2	−137
Aug-06	5.9	−52	Apr-09	1.3	−81
Sep-06	1.4	na[a]	May-09	2.1	−55
Oct-06	1.7	−89	Jun-09	2.7	−71
Nov-06	0.5	−94	Jul-09	4.0	−45
Dec-06	1.6	−104	Aug-09	1.7	−42
Jan-07	1.1	−105	Sep-09	2.0	−67
Feb-07	0.5	−131	Oct-09	1.9	−92
Mar-07	1.2	−63	Nov-09	0.3	−68
Apr-07	0.7	−85	Dec-09	1.3	−101
May-07	1.7	−45	Jan-10	1.3	−107
Jun-07	1.3	−45	Feb-10	1.2	−148
Jul-07	1.9	−58	Mar-10	1.0	−104
Aug-07	2.9	−58	Apr-10	1.4	−75
Sep-07	4.4	−42	May-10	1.1	−41
Oct-07	0.3	−61	Jun-10	0.6	−70
Nov-07	1.6	−127	Jul-10	4.1	−55
Dec-07	2.7	−76	Aug-10	3.4	−56
Jan-08	1.4	−112	Sep-10	1.3	na[a]
Feb-08	1.1	−121	Oct-10	2.1	−122
Mar-08	0.5	−135	Nov-10	0.0	−141
Apr-08	0.1	−132	Dec-10	1.2	−154
May-08	1.7	−111			

[a] Not measured.

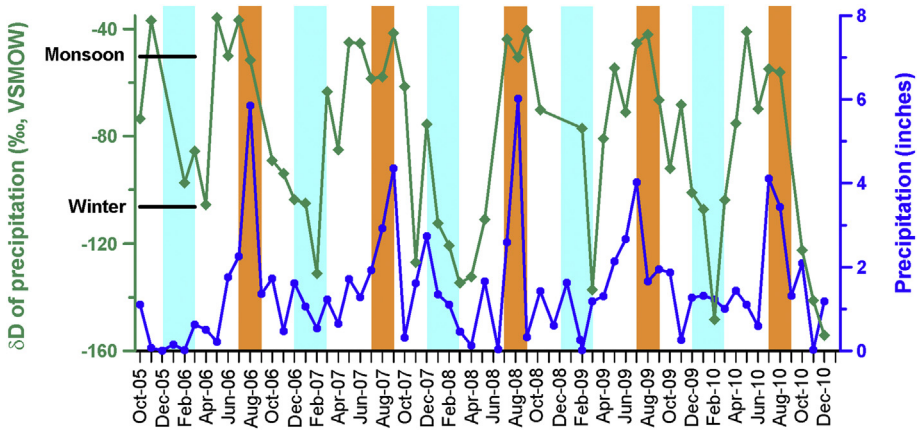

Fig. 2. Monthly δD values of precipitation (green line) and precipitation amount (blue line) from 2005 to 2010 in Valles Caldera, New Mexico. δD values were measured at GGRL (VSMOW, Vienna Standard Mean Ocean Water) and precipitation amount was measured at a nearby meteorological station. Summer (monsoonal) and winter months are highlighted in orange and green shades respectively. The weighted mean δD values during monsoon and winter seasons are shown on the left. (For interpretation of the references to color in this figure legend, the reader is referred to the web version of this article.)

weighted means using data on precipitation amount measured at a nearby meteorological station (35°N, 106°W; 2263.4 m a.s.l.) at LANL (Table 1; Fig. 2).

2.4. Reconstruction of the δD value of precipitation during the time span of the VC-3 core

2.4.1. Using the δD value of C_{28} n-alkanoic acid

δD values of terrestrial plant waxes, which comprise a variety of compounds including *n*-alkanes and *n*-alkanoic acids (Eglinton and Hamilton, 1967), have been found to track closely the δD value of local precipitation across transects in the US and Europe (Sachse et al., 2004, 2006; Shuman et al., 2006; Hou et al., 2008). Hou et al. (2008) found the correlation to be robust ($r^2 = 0.84$) particularly in dry regions of the southwestern US despite variations in precipitation amount, relative humidity and vegetation type, suggesting that the main controlling factor on the δD value of plant leaf waxes was the source of precipitation. Using surface sediments from a transect across Arizona and most of New Mexico (westward of 104.5°W) and local precipitation data obtained from Online Isotopes in Precipitation Calculator (OIPC, Bowen and Revenaugh, 2003), Hou et al. (2008) found a strong correlation between the δD value of C_{28} *n*-alkanoic acid extracted from the sediments and the weighted average δD of local precipitation as $\delta D\ C_{28} = 1.81^{*}\delta D_{prec} - 35.6$ (equation (1); $r^2 = 0.84$, $n = 18$, $p < 0.001$, residual mean squares (RMS) = 70.2).

Because the southwestern US transect studied by Hou et al. (2008) is relevant to the location of the VC-3 core, we applied equation (1) to the δD values of C_{28} *n*-alkanoic acid measured in our study and solved for δD_{prec} in order to reconstruct the δD value of precipitation during the time span of the Valles Caldera core (VC-3 δD_{prec}). To estimate the error in VC-3 δD_{prec}, we first calculated the standard error of the estimate (δD C_{28}) in the regression (equation 1) based on the precipitation data (δD and amount) used by Hou et al. (2008). We estimated the standard error of δD C_{28} in equation (1) to be ±12‰, which translates in ±7‰ error in our estimates of VC-3 δD_{prec} using equation (1).

2.4.2. Using the apparent isotopic fractionation factor (ε)

As a comparison to the C_{28} *n*-alkanoic acid-based reconstruction, we reconstructed VC-3 δD_{prec} based on the apparent fractionation factor between the δD value of C_{28} *n*-alkanoic acid and the δD of precipitation. Hydrogen isotopic fractionation results from soil water evaporation and leaf water transpiration and from biosynthesis of plant waxes. The combined effect of these processes results in a different hydrogen isotopic composition of plant leaf waxes with respect to that of precipitation and is referred to as the apparent fractionation factor. Evapotranspiration effects lead to isotopic enrichment (Leaney et al., 1985; Yakir et al., 1990) and different plant types can have different δD values of leaf waxes under the same environmental conditions (Hou et al., 2007; Pedentchouk et al., 2008). Hence the value of the isotopic fractionation depends strongly on vegetation type and environmental conditions (relative humidity, temperature). Nevertheless, it has been shown that the apparent isotopic fractionation between the δD of plant leaf waxes and the δD of precipitation is controlled by the opposing isotopic effects of relative humidity (RH) and vegetation assemblages (Hou et al., 2008; Gao et al., 2014), resulting in a net apparent fractionation not dominated by either effect. Relevant to this study is the apparent fractionation factor found by Hou et al. (2008), which remained relatively constant across the southwestern US transect, despite changes in RH and vegetation type. We have used the average fractionation factor for the southwestern US transect (−98.8 ± 7.8‰; Hou et al., 2008) to obtain a second reconstruction of the VC-3 δD_{prec} and we estimated the associated error by error propagation.

2.5. Correction for ice volume during glacial periods

All the reconstructed δD values of precipitation during glacial periods were corrected for the effect of ice volume on the isotopic content of meteoric water. We used the global benthic $\delta^{18}O$ record (Lisiecki and Raymo, 2005) to estimate the $\delta^{18}O$ shift in sea water at the age intervals of our reconstructed δD values and applied the 8‰ slope from the global meteoric water line (Craig, 1961) to estimate the corresponding shift in the δD value of precipitation. Correction factors shifted δD values by −11 to −8‰ during MIS 10 and by −13 to −5‰ during MIS 12.

3. Results and discussion

3.1. δD value of C_{28} n-alkanoic acid extracted from the VC-3 core

δD C_{28} values exhibit major cycles of 40–50‰ in amplitude during MIS 11 and at the onset of MIS 13 that are absent during glacial periods (Fig. 3; Table 2), variability during MIS 14 is the

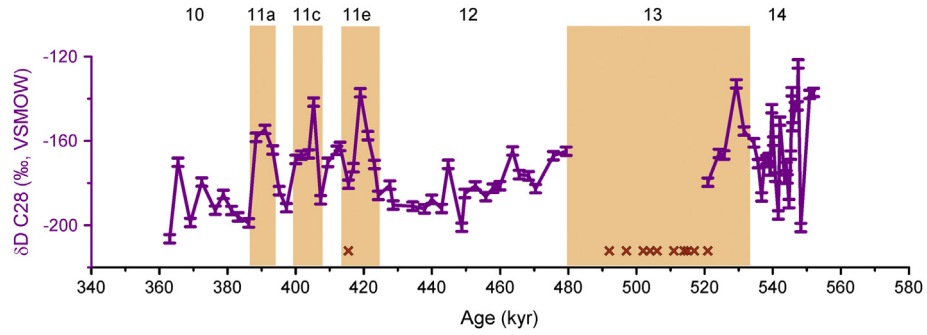

Fig. 3. δD values of C_{28} *n*-alkanoic acid measured in the Valles Caldera core (2‰ analytical error shown). Numbers 10 to 14 indicate marine isotope stages (MIS), shaded areas indicate interglacials 11 and 13 including warm substages within MIS 11 (a, c and e) (Fawcett et al., 2011). Brown crosses indicate the location of mud cracks in the VC-3 core. (For interpretation of the references to color in this figure legend, the reader is referred to the web version of this article.)

Table 2
δD value of C_{28} *n*-alkanoic acid measured in VC-3 core and reconstructed δD of precipitation (VC-3 δD_{prec}) based on the δD value of C_{28} *n*-alkanoic acid (Hou et al., 2008, Eq. 1) and based on the apparent fractionation factor (ε) between the δD of plant leaf waxes and the δD of precipitation in the region (Hou et al., 2008).

Age (ka)	δD of C_{28} *n*-alkanoic acid	VC-3 δD_{prec} (‰) δD_{C28}-based	VC-3 δD_{prec} (‰) ε-based	Age (ka)	δD of C_{28} *n*-alkanoic acid	VC-3 δD_{prec} (‰) δD_{C28}-based	VC-3 δD_{prec} (‰) ε-based
363.00	−206	−106	−119	466.95			
365.44	−170	−85	−82	468.30	−177	−86	−86
369.08	−199	−100	−110	469.23			
372.43	−180	−90	−91	470.38	−183	−88	−91
376.39	−193	−96	−103	474.22			
378.76	−185	−91	−95	475.60	−167	−80	−75
381.17	−193	−95	−103	477.51			
383.10	−196	−97	−105	479.34	−165	−77	−71
386.23	−199	−90	−100	481.47			
388.35	−158	−68	−60	496.92			
390.98	−155	−66	−56	511.17			
393.26	−164	−71	−66	520.96	−180	−80	−81
395.16	−184	−82	−85	522.09			
397.28	−192	−86	−93	523.18			
400.05	−169	−74	−70	524.24	−166	−72	−67
401.70	−167	−72	−68	525.71	−167	−72	−68
403.86	−166	−72	−67	529.31	−133	−54	−34
405.28	−142	−59	−43	531.59	−155	−66	−57
407.33	−188	−84	−89	534.46	−161	−69	−62
409.46	−170	−74	−71	535.74	−171	−75	−72
412.10	−165	−71	−66	536.75	−187	−83	−88
413.04	−163	−70	−64	537.53	−170	−74	−72
415.50	−181	−80	−82	538.22	−169	−74	−70
416.94	−173	−76	−74	538.86	−168	−73	−69
418.97	−137	−56	−38	539.23	−174	−77	−76
421.21	−158	−67	−59	539.74	−145	−60	−46
423.13	−171	−75	−72	540.21	−160	−69	−61
424.28	−186	−83	−87	540.79	−177	−78	−78
427.66	−181	−80	−82	541.15			
428.63	−190	−96	−102	541.65	−195	−88	−96
434.38	−191	−99	−105	542.13	−151	−64	−52
437.84	−192	−98	−105	543.53	−178	−79	−79
439.95	−188	−95	−100	544.01	−172	−75	−73
442.86	−192	−98	−105	544.28	−178	−79	−79
444.80	−171	−86	−83	544.78	−190	−85	−91
448.78	−201	−102	−113	545.30	−167	−72	−68
449.68	−185	−93	−96	545.64	−137	−56	−38
452.69	−181	−91	−93	545.79	−153	−65	−55
455.73	−186	−91	−95	546.58	−144	−60	−45
457.85	−182	−90	−93	547.26	−143	−60	−45
459.89	−181	−89	−91	547.47	−124	−49	−25
461.86				548.25	−201	−91	−102
463.63	−165	−81	−75	550.85	−138	−57	−39
464.84				552.00	−137	−56	−38
465.57	−176	−86	−86				

result of different factors, see below. Each of the major cycles observed during MIS 11 falls within the warm substages 11a, c and e (Fawcett et al., 2011), and a relatively smaller cycle is also observed during the cooler substage MIS 11d (Fig. 3). Interglacial periods are characterized by 20–30‰ higher δD C_{28} values on average relative to glacial periods. Note that average conditions for glacial periods are calculated for MIS 12 and 10, because MIS 14 corresponds to the initial formation and development of the lake. This section of the

core has the highest sedimentation rates and contains thick turbidites, gravels and silty muds (Fawcett et al., 2007) hence the large variability in the δD C_{28} values of this section of the record has local, environmental controls superimposed on glacial climate forcing.

3.2. The δD value of precipitation during MIS 13 to MIS 10

The δD value of precipitation reconstructed using equation (1), shows similar variation to the δD values of C_{28} *n*-alkanoic acid with major cycles of 20–30‰ amplitude during interglacials MIS 11 and MIS 13 and lower values without predominant cycles during glacial periods (Fig. 4A; Table 2). Overall, the VC-3 δD_{prec} values range from −53.8‰ to −94.4‰, with a mean value of −77.5 ± 8‰. Remarkably, this variation falls within the present-day summer monsoonal and winter weighted means (−50.3 ± 3‰ and −106.4 ± 20‰ respectively), suggesting that processes similar to those of present time also controlled precipitation during MIS 13 to 10. The second reconstruction of VC-3 δD_{prec} using the apparent fractionation factor (Section 2.4.2.) results in similar variability and overall values through the record with cycles during interglacials of relatively greater amplitude (40‰; Fig. 4B; Table 2). This similarity between the two reconstructions is expected as each are based on correlations of the same precipitation and δD_{wax} data (Hou et al., 2008). However, the remarkable agreement of these reconstructions with measured modern mean δD values of precipitation was not expected given the different time scales between the data used by Hou et al. (2008), which may cover decades at the most in the surface sediments sampled, and the time scale of the VC-3 core, which spans thousands of years at our sampling resolution.

The VC-3 δD_{prec} records shows similarities with the global benthic $\delta^{18}O$ record (Lisiecki and Raymo, 2005) and the δD record from the Antarctic Dome C ice core (Jouzel et al., 2007) (Fig. 4C and D). In addition to the characteristic glacial–interglacial contrast, the VC-3 δD_{prec} records shows the progressively decreasing (cooling) trend during MIS 12 and the abrupt increase (warming) at the onset of MIS 11 (Fig. 4). These similarities illustrate the influence of global scale forcing on precipitation changes in the southwestern US. However, differences from the benthic $\delta^{18}O$ and Antarctic Dome C ice core records also exist. For instance, the onset of MIS 13 in the benthic and Antarctic records is less pronounced relative to MIS 11. Similarity in intensity between the onsets of these interglacials has been observed in other regions of Asia and Europe (Yin and Guo, 2008). The most prominent features in the VC-3 δD_{prec} records, which do not exist in the benthic $\delta^{18}O$ and Antarctic Dome C ice core records are the distinct cycles during interglacials MIS 11 and 13. This feature suggests the important influence of a regional climate forcing on precipitation changes in the southwestern US during these interglacials.

3.3. Regional factors influencing the δD value of precipitation

Regional variables that can influence the δD value of precipitation are: (1) evaporation, which results in higher δD values of precipitation, (2) amount of precipitation (amount effect), which results in lower δD values with greater precipitation and (3) changes in precipitation sources that have different δD values. Evaporative conditions were the strongest during MIS 11e and late MIS 13 (Fawcett et al., 2011) and therefore may have contributed to the highest values observed in VC-3 δD_{prec} during MIS 11e but not elsewhere in the record. At present, the amount effect is not observed in the δD of precipitation in the region (Fig. 5). In addition, in the VC-3 δD_{prec} records, the presence of mud cracks in the core, which are times of reduced precipitation, coincide with times of minimum δD_{prec} values during late MIS 11e (Fig. 4A) and this argues against an amount effect (lower δD_{prec} values due to greater precipitation) during this period and elsewhere were δD_{prec} values are low.

Changes in the source/pathways of water masses delivering precipitation with different δD values could have contributed to the

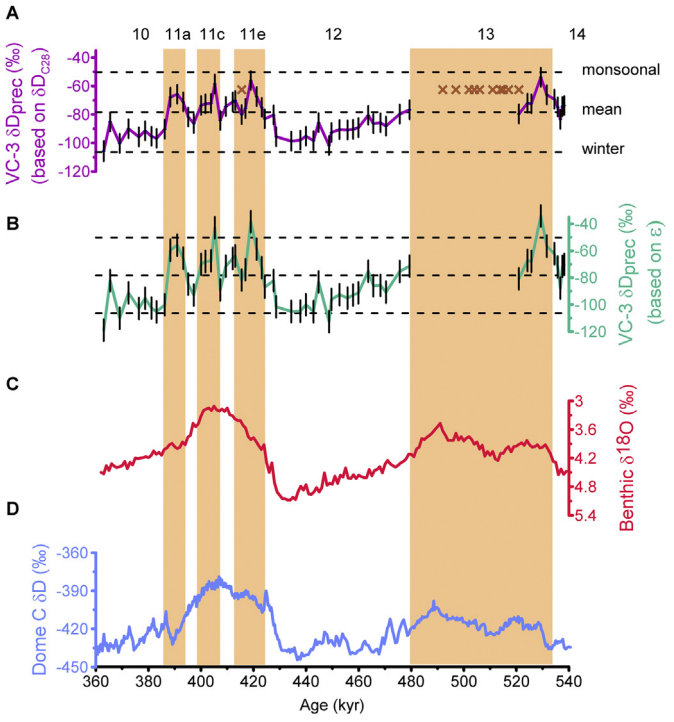

Fig. 4. Reconstructions of the δD record of precipitation during the time span of the VC-3 core (VC-3 δD_{prec}) in Valles Caldera, New Mexico compared to global records. A) Reconstruction based on the δD value of C_{28} *n*-alkanoic acid (Hou et al, 2008), dotted lines show the modern mean values for summer monsoonal (July–September) and winter (December–March) precipitation in the region. B) Reconstruction based on the apparent fractionation factor (ε) between the δD of plant leaf waxes and the δD of precipitation in the region (Hou et al., 2008), dotted lines show modern mean monsoonal and winter values as above. C) Benthic $\delta^{18}O$ record (Lisiecki and Raymo, 2005), and D) Antarctic δD values from Dome C ice core (Jouzel et al., 2007). Numbers 10–14 indicate Marine Isotope Stages (MIS), shaded areas outline interglacials 11 and 13 including warm substages within MIS 11 (a, c and e) (Fawcett et al., 2011). Brown crosses indicate the location of mud cracks in the VC-3 core. (For interpretation of the references to color in this figure legend, the reader is referred to the web version of this article.)

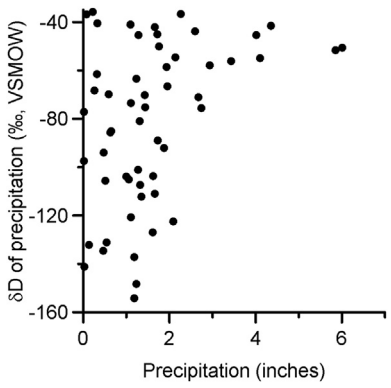

Fig. 5. δD value of precipitation vs. precipitation amount in Valles Caldera, New Mexico at present. Monthly δD values of precipitation were measured at the GGRL (VSMOW, Vienna Standard Mean Ocean Water) and monthly precipitation amount was measured at a nearby meteorological station. Data spans a 5-year period (2005–2010).

variability in the VC-3 δD_{prec} records. At present, such changes occur with season in the region. During the summer, monsoonal precipitation originates from the Gulf of California and the Gulf of Mexico whereas winter precipitation originates from the North Pacific (Schmitz and Mullen, 1996; Friedman et al., 2002; Xu et al., 2004; Cerezo-Mota et al., 2011). These dominant sources delivering precipitation to the region represent the greatest annual variability in the δD value of precipitation annually, with higher values during the summer monsoon (Fig. 2). The fact that similar variability in δD values of precipitation is evident during interglacials MIS 13 and 11 (albeit averaged over a larger timescale), suggests similar patterns of warm versus cool sources of precipitation during these interglacials. In addition, the remarkable agreement between the reconstructed Pleistocene δD values and the modern δD values in the region, suggests that atmospheric circulation patterns similar to those during modern summer and winter seasons governed sources of precipitation during warm and cool substages of interglacials MIS 13 and 11.

3.4. Monsoonal/warm precipitation sources during Pleistocene interglacials

If the modern dominant sources of precipitation in the southwestern US during warm and cool seasons were similarly dominant during warm and cool substages of interglacials MIS 11 and 13, we can interpret the variability in the VC-3 δD_{prec} records as an indicator of monsoon strength, particularly during interglacials (see below). This interpretation assumes that modern atmospheric patterns are comparable to atmospheric patterns during interglacials MIS 13 and 11. This assumption is reasonable based on 1) the remarkable agreement between our reconstructed δD values of precipitation and the modern seasonal δD values of precipitation, as mentioned above, (Fig. 4A) and 2) the similarities between MIS 11 and the current interglacial in terms of insolation and MAT's (Fawcett et al., 2011), whereas for MIS 13, the early part of this interglacial in the VC-3 δD_{prec} records suggests some similarity existed in atmospheric patterns between MIS 11 and 13.

During glacial periods, low δD values in the reconstructed VC-3 δD_{prec} records agree with a predominantly winter source of precipitation however the assumption of similarity in atmospheric patterns to present time is not necessarily applicable. During glacial periods, atmospheric circulation over North America and resulting moisture sources to the southwestern US were likely different than those prevailing during interglacial periods. Full glacial conditions including the extension of the continental ice sheets 10° further south, the southward displacement of the jet stream across the Pacific and a weaker subtropical high over the Pacific combined to cause colder climate, colder surface ocean temperatures and different surface wind fields than those during interglacial times (COHMAP, 1988). Glacial conditions likely favored a larger contribution of moisture source from Northern Pacific in the form of winter precipitation in the southwest with relatively less precipitation during the summer (COHMAP, 1988; Imbrie et al., 1983). Consequently, warm summer precipitation sources derived from the Gulf of Mexico and California were likely diminished during glacial periods. Nevertheless, the lower reconstructed values in the VC-3 δD_{prec} record during glacials MIS 12 and 10 with respect to interglacials MIS 13 and 11 (Fig. 4A) are consistent with a predominantly winter source of precipitation, similar to modern winter δD values.

Unfortunately, it is not possible to precisely quantify the relative proportion of monsoonal/warm precipitation during the time span of the VC-3 core using the VC-3 δD_{prec} records. At present, ~50% of annual precipitation is from summer monsoonal sources (Douglas et al., 1993). We attempted to reproduce this proportion by using the modern 5-yr data set of precipitation amount and δD values (Table 1; Fig. 2). Choosing the maximum and minimum δD values as end-members (representative of warm and cold precipitation respectively), we reproduced an average of 60% monsoonal contribution annually. However, due to the natural monthly variability in the δD values, there is an uncertainty of ~30% in the estimates (Table 3). Therefore, we opted for not applying this approach to the VC-3 core data and instead interpret the record semi-quantitatively.

The VC-3 δD_{prec} records undoubtedly reveal considerable variation in monsoon strength in the southwestern US during interglacial periods MIS 13 and 11. During MIS 11, greater monsoon strength occurred during the warmest periods during substages 11a, c and e (Fig. 6A) whereas the opposite is true during cool substages. Several lines of evidence support our interpretation of monsoon strength and its variability. First, the glacial–interglacial variation is consistent with the fact that interglacial conditions would have provided an optimal differential heating of land versus ocean surface similar to the early Holocene (Liu et al., 2003). Second, the correspondence between variations in monsoon strength and variations in independent proxies of ecosystem productivity, namely TOC, $\delta^{13}C_{TOC}$ and Si/Ti ratio (Fig. 6B, C and D; Fawcett et al., 2011) confirms the monsoonal estimates. The association between strong monsoonal precipitation and increased terrestrial and aquatic productivity during interglacials is suggested by the concomitant increase in monsoonal strength and TOC, an indicator of organic matter inputs from land and/or production within the lake. Similarly, increases in $\delta^{13}C_{TOC}$, which suggests an expansion of terrestrial plants with high water use efficiency, e.g. C4 plants, and/or an increase in aquatic productivity in the lake (Meyers, 2003), parallel times of strong monsoon (Fig. 6C). The presence of C4 grasses would have been favored during interglacials due to the warmer and drier climate relative to glacial periods. Lastly, increases in Si/Ti, an indicator of aquatic productivity, coincide with increased monsoon precipitation during interglacials MIS 13 and 11 (Fig. 6D).

In addition, it is notable that during MIS 11e, the strength of the monsoon reached a maximum but collapsed later during this warm substage. The presence of mud cracks in the core during late MIS 11e coinciding with the collapse of the monsoon is another independent corroboration of our estimates. Furthermore, according to our interpretation based on the VC-3 δD_{prec} records, times of greater monsoon strength are positively correlated to mean annual temperature (MAT) and warm pollen taxa *Juniperus* and *Quercus* (Fig. 6E, F and G; Fawcett et al., 2011). The correspondence between each of these independent proxies and monsoon strength in the southwestern US, provides further confidence on the reconstruction of precipitation changes based on the δD value of sedimentary plant leaf waxes in the Valles Caldera sedimentary archive.

3.5. Factors influencing monsoon strength

Some correspondence exists between maximum monsoon strength and insolation maxima at 30°N, particularly during MIS 13

Table 3
Estimates of the average annual proportion of summer monsoonal precipitation at present using modern seasonal mean δD values as end-members (see Section 3.4).

Year	Proportion	Standard deviation
2006	0.67	0.24
2007	0.67	0.26
2008	0.54	0.33
2009	0.66	0.23
2010	0.48	0.34
5-yr	0.61	0.28

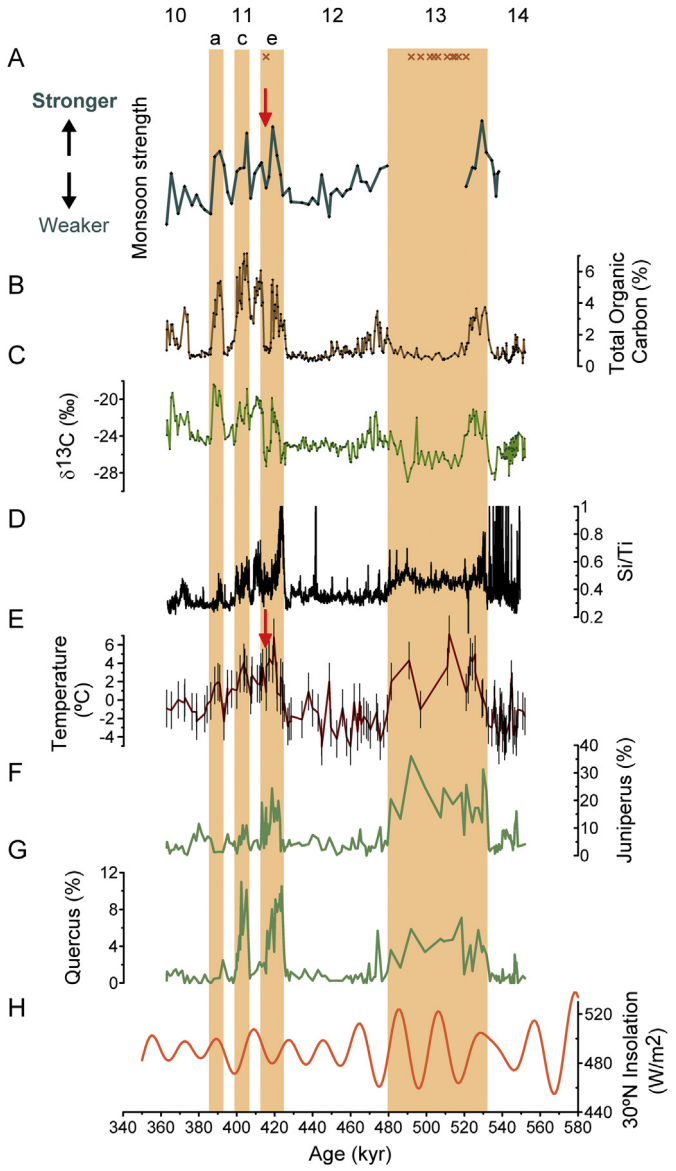

Fig. 6. Relative monsoon strength in Valles Caldera, New Mexico during the late Pleistocene compared to independent proxies measured in the VC-3 core (Fawcett et al., 2011) and insolation changes. A) Relative monsoon strength in Valles Caldera, New Mexico, estimated based on the δD record of precipitation (VC-3 δD_{prec}) reconstructed using the δD value of C_{28} *n*-alkanoic acid (Hou et al, 2008; Eq. 1). B) Total organic carbon (TOC). C) $\delta^{13}C$ of TOC. D) Si/Ti. E) Mean annual temperature (MAT). F) Juniperus abundance. G) Quercus abundance. H) Mid-June insolation at latitude 30°N (Berger and Loutre, 1991). Numbers 10–14 indicate Marine Isotope Stages (MIS), shaded areas outline interglacials 11 and 13 including warm substages within MIS 11 (a, c and e) (Fawcett et al., 2011). Red arrows in late MIS 11e highlight minimum monsoonal precipitation during relatively high MATs. Brown crosses indicate the location of mud cracks in the VC-3 core. (For interpretation of the references to color in this figure legend, the reader is referred to the web version of this article.)

and during the second half of MIS 11, with lags of ~5 ka during the first half of MIS 11 (Fig. 6A and H). The association between monsoon intensity and insolation changes has been reported for the Asian Monsoon (Nakagawa et al., 2008). Similarly, several studies have reported a low-latitude precessional forcing of climate variability, including monsoonal precipitation (Short et al., 1991; Hagelberg et al., 1994; McIntyre and Molfino, 1996; Clemens and Tiedemann, 1997; Niemitz and Billups, 2005; Wang et al., 2008; Weirauch et al., 2008). Temperature and precipitation response to maximum insolation can be transferred to higher latitudes via atmospheric circulation (Short et al., 1991; McIntyre and Molfino, 1996) whereas precessional forcing of equatorial climate associated with the Milankovitch theory (Berger, 1988) has been observed in sedimentary records from the equatorial Pacific and the Atlantic (Hagelberg et al., 1994; Clemens and Tiedemann, 1997; Niemitz and Billups, 2005; Weirauch et al., 2008) and in climate simulations (Short et al., 1991).

At interannual time scales, variations in monsoon strength are explained by the land-sea surface temperature contrast (LSTC), which drives the onset of the North American Monsoon (Zhu et al., 2007) and the initial monsoon intensity (Turrent and Cavazos, 2009). We expect a similar scenario during interglacial periods MIS 13 and 11 in the southwestern US. MAT increases ranging from 4 °C to 9 °C during these interglacials (calibration error in MAT values is estimated as ~2 °C; Fawcett et al., 2011) suggest similar increases in land surface temperature (Fig. 6E). In contrast, increases in sea surface temperatures should be expected to be relatively smaller, given the greater heat capacity of the ocean with respect to land. The influence of a stronger LSTC, resembling the MAT record, is observed during MIS 11 and this influence likely existed to some degree during MIS 13 (Fig. 6A and E). However, during the latter part of MIS 11e, monsoonal precipitation collapsed while LSTC would have remained strong based on the relatively warm MAT values (Fig. 6A and E). The fact that this minimum in monsoonal precipitation occurred during the warmest interval of the interglacial suggests a collapse of the monsoon system caused by a threshold level of warming. Suppression of monsoonal precipitation by significant warming could occur as a result of reduced soil moisture (due to enhanced evaporation) and atmospheric stability (Cook and Seager, 2013). The monsoon collapse during the latter part of MIS 11e was characterized by severe aridity (as evidenced by the presence of mud cracks in the core), unlike other times of monsoon minima during MIS 11. Note that other times of monsoon minima during MIS 11 occurred during the cooler substages 11b and d (MATs ~0–2 °C; Fig. 6A and E) and preservation of soil moisture and the winter contribution to annual precipitation may have prevented severe aridity. Similarly, we suggest that the prolonged arid period during MIS 13 resulted from the combined effect of warming (highest temperatures occurred at ~512 ka) and the collapse of the monsoon system although additional measurements are needed to confirm this. Periods of minimum monsoonal precipitation following/during the warmest period of the interglacial, such as during MIS 11e, may represent a natural example of the projected droughts in the region, which are underlined by more complex forcing involving changes in atmospheric circulation (Seager et al., 2007). Recent climate simulations also suggest that greenhouse gas warming could cause a change in the timing of the monsoon system although an overall reduction in annual rainfall is still predicted (Cook and Seager, 2013). Although the temporal resolution in the VC-3 record is coarser than that of model studies, the VC-3 record provides the variability in monsoonal precipitation over a much larger timescale than that of model-based studies (millennia vs. centennial respectively) and it clearly shows that monsoon strength can weaken significantly during interglacial periods. In addition, it shows the decline in monsoon strength concomitant with times of sustained aridity as seen during the latter part of MIS 11e. This arid period could be considered an analog for present climate based on the time elapsed since the onset of the current interglacial (~10–12 ka) and insolation similarities between the current interglacial and MIS 11. It follows that, at present, the region is under a state of weakened monsoon precipitation and consequent aridity but that some recovery of the monsoon system could gradually occur over the next millennia (based on the current sampling resolution in the VC-3 record).

However, the effects of anthropogenic warming could enhance the persistence of drought (Cook et al., 2013), meaning that the natural cycles in monsoon strength shown in the VC-3 record could be disrupted.

4. Conclusions

We reconstructed the δD value of precipitation during MIS 13 to the onset of MIS 10 in northern New Mexico using the δD values of sedimentary C_{28} *n*-alkanoic acid, as in the correlation by Hou et al. (2008) and the reported fractionation factor between the δD of plant leaf waxes and the δD of precipitation (Hou et al., 2008). The reconstructed δD values are in agreement with modern δD summer monsoonal and winter annual values, suggesting similar atmospheric processes to present time were in place, particularly during interglacials MIS 13 and 11. Based on the δD summer monsoonal and winter mean values as end-members and the widely accepted correlation between the δD of plant leaf waxes and the δD of precipitation, we interpret our reconstructed δD records of precipitation as a proxy for monsoon strength during the time span of the VC-3 core. Interglacial periods were characterized by greater monsoon strength but also greater variability compared to glacial periods. Pronounced cycles of monsoonal strength occurred during interglacial periods and during MIS 11 in particular, maxima occurred during the warmest substages 11a, c and e (Fig. 6A) with minimum strength occurred during cooler substages. Our estimates are in agreement with MAT values, warm pollen taxa *Juniperus* and *Quercus* and proxies of ecosystem productivity, namely, TOC, $\delta^{13}C_{TOC}$ and Si/Ti ratio. The variation in monsoon strength seems to follow insolation and temperature changes, and less variability is found during glacial MIS 12. However, the association between strong monsoon and warm temperatures breaks down during the early part of MIS 11, when monsoonal strength decreases to a minimum while MATs and likely LSTC remained relatively high. The severe drought identified during this interval based on mud-cracks in the lake core (Fawcett et al., 2011) suggests that reduction in monsoonal precipitation played an important role in the onset of drought. Similarly, our estimates suggest that the extended period of mud-cracks during MIS 13 (Fawcett et al., 2011) had significant reductions in monsoonal precipitation.

Our semi-quantitative assessments of the strength of the North American Monsoon during late Pleistocene interglacials constitute a record of natural variability in precipitation in the southwestern US. Of particular relevance to future climate in the region is MIS 11, which is generally considered an analog to the current interglacial in terms of MAT and insolation similarities. Based on our estimates, periods of low monsoonal precipitation can be induced by natural variability. However, our monsoonal record also suggests a threshold level of warming above which a more complex forcing drives monsoon intensity to a minimum, leading to aridity. This relation could have serious implications for future climate in the region as a result of human-induced warming.

Acknowledgments

We thank LRC/LacCore for assistance with core sampling. We thank two anonymous reviewers for their helpful comments on this manuscript. This work was supported by the NSF P2C2, IGPP LANL and the USGS Western Mountain Initiative.

References

Berger, A., 1988. Milankovitch theory and climate. Rev. Geophys. 26, 624–657.
Berger, A., Loutre, M.F., 1991. Insolation values for the climate of the last 10 million Years. Quat. Sci. Rev. 10, 297–317.
Bowen, G.J., Revenaugh, J., 2003. Interpolating the isotopic composition of modern meteoric precipitation. Water Resour. Res. 39 http://dx.doi.org/10.1029/2003WR002086.
Cerezo-Mota, R., Allen, M., Jones, R., 2011. Mechanisms controlling precipitation in the Northern Portion of the North American Monsoon. J. Clim. 24, 2771–2783. http://dx.doi.org/10.1175/2011JCLI3846.1.
Clemens, S.C., Tiedemann, R., 1997. Eccentricity forcing of Pliocene early Pleistocene climate revealed in a marine oxygen-isotope record. Nature 385, 801–804.
COHMAP Members, 1988. Climatic changes of the last 18,000 years: observations and model simulations. Science 241, 1043–1052.
Cook, E.R., Seager, R., Cane, M.A., Stahle, D.W., 2007. North American drought: reconstructions, causes, and consequences. Earth-Sci. Rev. 81, 93–134.
Cook, B.I., Seager, R., 2013. The response of the North American Monsoon to increased greenhouse gas forcing. J. Geophys. Res. Atmos. 118, 1690–1699.
Cook, B.I., Seager, R., Miller, R.L., Mason, J.A., 2013. Intensification of North American megadroughts through surface and dust aerosol forcing. J. Clim. 26, 4414–4430.
Coplen, T.B., Winograd, I.J., Landwehr, J.M., Riggs, A.C., 1994. 500,000-year stable carbon isotopic record from Devils Hole, Nevada. Science 263, 361–365.
Craig, H., 1961. Isotopic variations in meteoric waters. Science 133, 1702–1703.
Douglas, M.W., Maddox, R.A., Howard, K., Reyes, S., 1993. The Mexican Monsoon. J. Clim. 6, 1665–1677.
Eglinton, G., Hamilton, R., 1967. Leaf epicuticular waxes. Science 156, 1322–1335.
Fawcett, P.J., Heikoop, J.M., Goff, F., Anderson, R.S., Donohoo-Hurley, L., Geissman, J.W., WoldeGabriel, G., Allen, C.D., Johnson, C.M., Smith, S.J., Fessenden-Rahn, J., 2007. Two middle Pleistocene glacial–interglacial cycles from the Valle Grande, Jemez Mountains, northern New Mexico. In: New Mexico Geological Society Guidebook, 58th Field Conference, Geology of the Jemez Mountains Region II, pp. 409–417.
Fawcett, P.J., Werne, J.P., Anderson, R.S., Heikoop, J.M., Brown, E.T., Berke, M.A., Smith, S.J., Goff, F., Donohoo-Hurley, L., Cisneros-Dozal, L.M., Schouten, S., Damste, J.S.S., Huang, Y., Toney, J., Fessenden, J., WoldeGabriel, G., Atudorei, V., Geissman, J.W., Allen, C.D., 2011. Extended megadroughts in the southwestern United States during Pleistocene interglacials. Nature 470, 518–521.
Friedman, I., Smith, G.I., Johnson, C.A., Moscati, R.J., 2002. Stable isotope compositions of waters in the Great Basin, United States 2. Modern precipitation. J. Geophys. Res. Atmos. 107 http://dx.doi.org/10.1029/2001JD000566.
Gao, L., Zheng, M., Fraser, M., Huang, Y., 2014. Comparable hydrogen isotopic fractionation of plant leaf wax *n*-alkanoic acids in arid and humid subtropical ecosystems. Geochem. Geophys. Geosyst. 15, 361–373. http://dx.doi.org/10.1002/2013GC005015.
Hagelberg, T.K., Bond, G., deMenocal, P., 1994. Milankovitch band forcing of submilankovitch climate variability during the Pleistocene. Paleoceanography 9, 545–558.
Hou, J., D'Andrea, W.J., Huang, Y., 2008. Can sedimentary leaf waxes record D/H ratios of continental precipitation? Field, model, and experimental assessments. Geochim. Cosmochim. Acta 72, 3503–3517.
Hou, J., D'Andrea, W.J., MacDonald, D., Huang, Y., 2007. Hydrogen isotopic variability in leaf waxes among terrestrial and aquatic plants around Blood Pond, Massachusetts (USA). Org. Geochem. 38, 977–984.
Imbrie, J., McIntyre, A., Moore Jr., T.C., 1983. The ocean around North America at the last glacial maximum (Chapter 12). In: Wright Jr., H.E., Porter, S.C. (Eds.), Late Quaternary Environments of the United States. The Late Pleistocene, vol. I. University of Minnesota Press, Minneapolis, pp. 230–236.
Jouzel, J., Masson-Delmotte, V., Cattani, O., Dreyfus, G., Falourd, S., Hoffmann, G., Minster, B., Nouet, J., Barnola, J.M., Chappellaz, J., Fischer, H., Gallet, J.C., Johnsen, S., Leuenberger, M., Loulergue, L., Luethi, D., Oerter, H., Parrenin, F., Raisbeck, G., Raynaud, D., Schilt, A., Schwander, J., Selmo, E., Souchez, R., Spahni, R., Stauffer, B., Steffensen, J.P., Stenni, B., Stocker, T.F., Tison, J.L., Werner, M., Wolff, E.W., 2007. Orbital and millennial Antarctic climate variability over the past 800,000 years. Science 317, 793–796.
Leaney, F.W., Osmond, C.B., Allison, G.B., Ziegler, H., 1985. Hydrogen-isotope composition of leaf water in C-3 and C-4 plants – its relationship to the hydrogen-isotope composition of dry-matter. Planta 164, 215–220.
Lisiecki, L.E., Raymo, M.E., 2005. A Pliocene–Pleistocene stack of 57 globally distributed benthic $\delta^{18}O$ records. Paleoceanography 20. http://dx.doi.org/10.1029/2005PA001164.
Liu, Z., Otto-Bliesner, B., Kutzbach, J., Li, L., Shields, C., 2003. Coupled climate simulation of the evolution of global monsoons in the Holocene. J. Clim. 16, 2472–2490.
McIntyre, A., Molfino, B., 1996. Forcing of Atlantic equatorial and subpolar millennial cycles by precession. Science 274, 1867–1870.
Meyers, P.A., 2003. Applications of organic geochemistry to paleolimnological reconstructions: a summary of examples from the Laurentian Great Lakes. Org. Geochem. 34, 261–289.
Nakagawa, T., Okuda, M., Yonenobu, H., Miyoshi, N., Fujiki, T., Gotanda, K., Tarasov, P.E., Morita, Y., Takemura, K., Horie, S., 2008. Regulation of the monsoon climate by two different orbital rhythms and forcing mechanisms. Geology 36, 491–494.
Niemitz, M.D., Billups, K., 2005. Millennial-scale variability in western tropical Atlantic surface Ocean hydrography during the early Pliocene. Mar. Micropaleontol. 54, 155–166.
Pedentchouk, N., Sumner, W., Tipple, B., Pagani, M., 2008. $\delta^{13}C$ and δD compositions of *n*-alkanes from modern angiosperms and conifers: an experimental setup in central Washington State, USA. Org. Geochem. 39, 1066–1071.

Sachse, D., Radke, J., Gleixner, G., 2004. Hydrogen isotope ratios of recent lacustrine sedimentary n-alkanes record modern climate variability. Geochim. Cosmochim. Acta 68, 4877–4889.
Sachse, D., Radke, J., Gleixner, G., 2006. δD values of individual n-alkanes from terrestrial plants along a climatic gradient – implications for the sedimentary biomarker record. Org. Geochem. 37, 469–483.
Schmitz, J.T., Mullen, S.L., 1996. Water vapor transport associated with the summertime North American monsoon as depicted by ECMWF analyses. J. Clim. 9, 1621–1634.
Seager, R., Kushnir, Y., Herweijer, C., Naik, N., Velez, J., 2005. Modeling of tropical forcing of persistent droughts and pluvials over western North America: 1856–2000. J. Clim. 18, 4065–4088.
Seager, R., Ting, M., Held, I., Kushnir, Y., Lu, J., Vecchi, G., Huang, H.-P., Harnik, N., Leetmaa, A., Lau, N.-C., Li, C., Velez, J., Naik, N., 2007. Model projections of an imminent transition to a more arid climate in southwestern North America. Science 316, 1181–1184.
Sears, P.B., Clisby, K.H., 1952. Two long climate records. Science 116, 176–178.
Short, D.A., Mengel, J.G., Crowley, T.J., Hyde, W.T., North, G.R., 1991. Filtering of Milankovitch cycles by Earth's geography. Quat. Res. 35, 157–173.
Shuman, B., Huang, Y., Newby, P., Wang, Y., 2006. Compound-specific isotopic analyses track changes in seasonal precipitation regimes in the Northeastern United States at ca. 8200 cal yr BP. Quat. Sci. Rev. 25, 2992–3002.
Turrent, C., Cavazos, T., 2009. Role of the land-sea thermal contrast in the interannual modulation of the North American Monsoon. Geophys. Res. Lett. 36 http://dx.doi.org/10.1029/2008GL036299.
Wang, Y., Cheng, H., Edwards, R.L., Kong, X., Shao, X., Chen, S., Wu, J., Jiang, X., Wang, X., An, Z., 2008. Millennial- and orbital-scale changes in the East Asian monsoon over the past 224,000 years. Nature 451, 1090–1093.
Weirauch, D., Billups, K., Martin, P., 2008. Evolution of millennial-scale climate variability during the mid-Pleistocene. Paleoceanography 23. http://dx.doi.org/10.1029/2007PA001584.
Winograd, I.J., Coplen, T.B., Landwehr, J.M., Riggs, A.C., Ludwig, K.R., Szabo, B.J., Kolesar, P.T., Revesz, K.M., 1992. Continuous 500,000-year climate record from vein calcite in Devils Hole, Nevada. Science 258, 255–260.
Xu, J., Gao, X., Shuttleworth, J., Sorooshian, S., Small, E., 2004. Model climatology of the North American monsoon onset period during 1980–2001. J. Clim. 17, 3892–3906.
Yakir, D., Deniro, M.J., Gat, J.R., 1990. Natural deuterium and O-18 enrichment in leaf water of cotton plants grown under wet and dry conditions – evidence for water compartmentation and its dynamics. Plant Cell Environ. 13, 49–56.
Yin, Q.Z., Guo, Z.T., 2008. Strong summer monsoon during the cool MIS-13. Clim. Past 4, 29–34.
Zhu, C., Cavazos, T., Lettenmaier, D.P., 2007. Role of antecedent land surface conditions in warm season precipitation over northwestern Mexico. J. Clim. 20, 1774–1791.